

LOW LOSS CIRCULAR BIREFRINGENCE IN ARTIFICIAL TRIPLE HELICES

Amornthep Sonsilphong and Nantakan Wongkasem*

Metasolver Laboratory, Department of Electrical Engineering, Faculty of Engineering, Khon Kaen University, Khon Kaen 40002, Thailand

Abstract—Low loss circular birefringence is found in three-dimensional artificial triple helices. High values of chirality index are generated. Within the transmission bandwidth, there is a significant difference in the refractive index value of the right- and left-circularly polarized waves. The outgoing waves from a wedge structure designed from these triple helices are proved to split with a wide angle. The wave polarizations agree with earlier simulation results.

1. INTRODUCTION

Helices are one of the well-known chiral structures found in several natural molecules, e.g., DNA, sucrose, proteins, etc., as well as solid elements such as quartz and crystal. Optical activity presented in helix structures in terms of chirality parameter, κ , has been reported [1, 2]. The chirality parameter based on the constitutive relations [3] describes the cross-coupling between electric and magnetic field. Due to optical activity or optical rotary dispersion (ORD), any arbitrary polarization wave splits into a right-circularly polarized (RCP) wave and a left-circularly polarized (LCP) wave with different phase velocity and different refractive index, i.e., n_+ of the RCP wave and n_- of the LCP wave, while propagating independently inside the chiral media. This double refraction of the circular polarized waves is also called circular birefringence from where the optical rotation is derived, as it rotates the plane of polarization of the polarized waves. The two circularly polarized waves are then coupled at the boundaries and exit the media in one polarization configuration, typically as an elliptically polarized

Received 25 January 2013, Accepted 8 March 2013, Scheduled 12 March 2013

* Corresponding author: Nantakan Wongkasem (nantakan@gmail.com).

wave, based on the absorption loss or circular dichroism (CD) of the media. The effective refractive index ($n_{eff} = (n_+ + n_-)/2$) of the chiral media is used to determine the direction of the leaving wave. However, the RCP and LCP waves can both continue to propagate outside the chiral media if the outgoing surface plane of the media is not perpendicular to the direction of the incoming waves. This can be done by constructing the media in different shapes, for instance in a wedge [4, 5] or triangle shape [6]. The two outgoing waves will propagate separately according to their refractive index generated earlier based on ORD. This wave/light splitting control is useful in beam splitters, polarizers, etc..

Artificial single and double helices have been proposed for broadband circular polarizers [7–9] and have improved the signal to noise ratio [10]. Multi-band circular polarizers using multilayered planar spiral metamaterials, where different transformation responses for the LCP and RCP waves were demonstrated, have been investigated [11, 12]. Chiral split-ring resonators (SRRs) formed in 3D double helix shape have been proposed as a resonant microwave absorber [13]. Several bi-layer and multi-layer chiral structures [14–17], as well as non-planar chiral SRRs [18] with strong optical activity and negative refractive index were studied in both microwave and optical regimes. Electromagnetic (EM) properties and negative refractive index of multiple helices, i.e., single, double, triple, quadruple, and quintuple helix were extensively studied [19]. High negative refractive index was found in three-dimensional double helices [20]. As the number of helical backbones increases it results in higher values of chirality index and lower loss [19]. The number of helical backbones is associated with an overlapping area of opposite handedness of the helix [21]. By changing the balance between left- and right-handed helices, the chirality index of the structures increases [22]. The chirality is also linked to transmission properties through the transmission phases [23].

This paper presents three-dimensional artificial triple helices where both RCP and LCP waves propagate inside the triple helix stack with low loss, unlike single and double helices, where one of the two circularly polarized waves is normally filtered out. The transmission coefficients and electromagnetic properties, i.e., refractive indices (n_+ , n_- and n_{eff}), chirality and loss factor are investigated. The 3D planar triple helices are fabricated and measured to validate the EM properties. The wedge design of these 3D triple helices is implemented to observe the circular birefringence. It has been found that these triple helices can generate wide splitting angle waves with low loss.

2. ARTIFICIAL HELICAL STRUCTURES

Three conventional helical structures, e.g., single, double, and triple helix, illustrated in Figures 1(a), 1(b), and 1(c), respectively, are initially investigated. Figure 1(d) shows the proposed 3D triple planar helix whose fabrication and testing is discussed in the next section. The geometric parameters of these helices are set as follows: pitch height, $H = 20$ mm and radius of wire, $R = 0.5$ mm. The transmission and reflection coefficients of these conventional helices are obtained by CST Microwave studio [24].

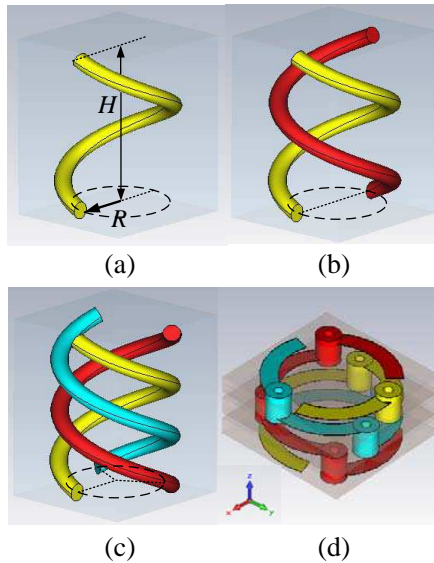


Figure 1. (Color online) conventional (a) single, (b) double, and (c) triple helix, (d) 3D triple planar helix.

The RCP and LCP waves are excited along the $-z$ direction. A periodic boundary is set on the $x-y$ plane and therefore the helices are seen as a periodic array on the $x-y$ plane with one row along the z axis. The effective refractive index, n_{eff} , chirality, $\kappa = (n_+ - n_-)/2$, and loss factor of RCP (LF_+) and LCP (LF_-), $LF_{\pm} = |\text{Im}(n_{\pm})/\text{Re}(n_{\pm})|$ are extracted from transmission and reflection coefficients [25] illustrated in Figure 2.

The transmission properties of single and double conventional helices indicate filter ability where an unwanted polarized wave can be eliminated. Based on its right-handed orientation, the RCP wave can propagate through both single and double helices, while the LCP wave

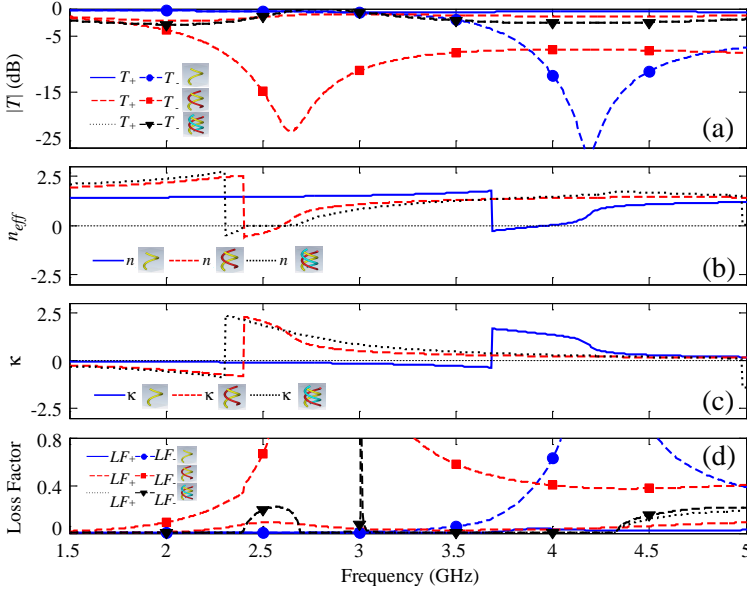


Figure 2. (Color online) (a) transmission coefficient: T_+ for RCP wave and T_- for LCP wave, (b) effective refractive index, (c) chirality and (d) loss factor: LF_+ for RCP wave and LF_- for LCP wave of single, double, and triple helix.

is almost blocked [7–10, 19] at the resonance frequency, at 4.20 GHz for single helix and 2.60 GHz for double helix. As the balance between left- and right-handed helices is improved, the triple helix allows both RCP and LCP waves to travel through. The transmission coefficient of both RCP and LCP waves is then enhanced. The amplitude of the RCP and LCP waves is almost identical, as shown in Figure 2(c). The low loss illustrated in the loss factor plot also supports this design. It is important to stress that all three helical structures can generate negative refractive index, which was also demonstrated in an earlier study [19].

3. THREE-DIMENSIONAL TRIPLE HELICES

The schematics of 3D planar triple helix chiral metamaterials are shown in Figure 3. The structures are fabricated on FR-4 boards. The dielectric constant of the FR-4 board is $\varepsilon = 4.3 + 0.23i$. The thickness of copper is 0.03 mm. CST Microwave Studio based on finite integration technique (FIT) is used to determine the reflection and transmission

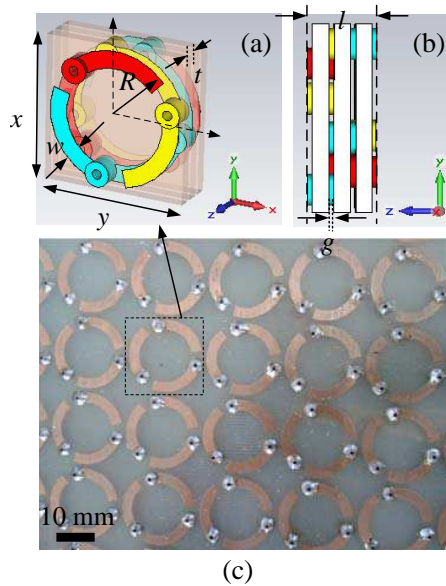


Figure 3. (Color online) a unit cell of 3D planar triple helix in (a) perspective, and (b) side view, and (c) a photograph of fabricated sample. The geometric parameters are: $x = y = 18.75$ mm, $w = 2.25$ mm, $l = 6.94$ mm, $g = 0.535$ mm, $R = 8.75$ mm, and $t = 1.6$ mm.

coefficients. Tetrahedral meshing is set in a frequency domain solver operating from 1.4 GHz to 3.0 GHz. The unit cell boundary condition of CST dictates the periodic orientation of the helices on the surface plane. The helix unit lattice is $18.75 \text{ mm} \times 18.75 \text{ mm} \times 6.94 \text{ mm}$. The right- and left-circularly polarized waves are excited along the $-z$ direction. The transmission and reflection coefficients obtained from the simulations are then used to retrieve other EM parameters [25].

Exactly the same material parameters and orientations used in fabricated helices are implemented throughout these EM full wave simulations. The ring with R radius is split into three equal arcs. An array of the three arcs is printed on each layer. At the adjacent layer, the array is rotated by 120° as illustrated in Figure 1(d). The arc from the previous layer is connected with the rotated arc (same color) of the neighboring layer through a created hole. To complete a helix pitch, these triple helices require four layers printed on three substrates. The diameters of the outer and inner hole are 3.25 mm and 1.25 mm respectively. Three FR4 substrates are used to complete a stack of arrays of one pitch triple helices. Figures 3(a) and 3(b)

illustrate the unit cell of 3D planar triple helix in a perspective view and side view. The 3D planar triple helices are manufactured with 10×10 unit cells. Some fabricated parts of the first layer are shown in Figure 3(c), where the dashed square indicates a unit cell of each helix. Note that to obtain multiple “ n ” backbone helices [11], there will be unconnected identical “ n ” arcs printed on each layer. Furthermore, the number of helix pitches can be increased by adding extra sets of multilayer stacks.

The reflection and transmission coefficients of the fabricated helix stack are measured by a vector network analyzer HP8753D. Horn antennas are used as transmitting and receiving ports. The vertical linear polarization waves are launched from the transmitter horn antenna through the helix stack and then are collected by the receiver horn in vertical and horizontal directions with a frequency step of 0.0125 GHz, from 1.4 GHz to 3.0 GHz. More details about the experiment procedure and setup can be found in an earlier report [20].

The transmission coefficients of RCP (T_+) and LCP (T_-) from the simulation and experiment are illustrated in Figure 4. The frequency is investigated in the 1.4 GHz–3.0 GHz range. The amplitude of the RCP and LCP waves has a similar pattern, illustrated in Figures 4(a) (simulation) and 4(b) (experiment), showing a pass band at the

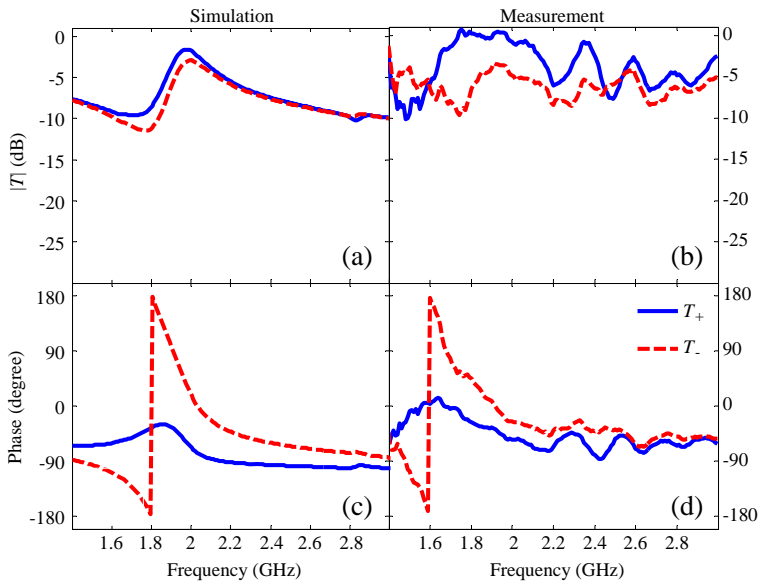


Figure 4. (Color online) simulation and experiment results of 3D planar triple helix: (a) and (b) transmission amplitude, (c) and (d) transmission phase from RCP and LCP excitation waves.

operating frequency from 1.8 GHz to 2.2 GHz. On the other hand, the phase of the RCP and LCP waves is different for both simulation (Figure 4(c)) and experiment (Figure 4(d)), confirming the chirality of the structures [23]. The effective refractive index and index of the RCP and LCP excitations, and chirality retrieved from the transmission and reflection coefficients [23, 25] are shown in Figures 5(a) (simulation) and 5(b) (measurement). The loss factor of RCP, LF_+ , and LCP, LF_- , and effective loss factor, LF_{eff} , are observed and presented in Figures 5(c) (simulation) and 5(d) (measurement).

The refractive index of the LCP wave, n_- , is negative from 1.80 GHz to 2.01 GHz (dash line, simulation) and from 1.60 GHz to 1.85 GHz (dash line, measurement), while the refractive index of the RCP wave, n_+ , (solid line, simulation) and the chirality, κ , (dashed-dotted line, simulation) are positive, as shown in Figure 5(a). As illustrated in Figure 5(b), κ from measured data is also positive from 1.60 GHz to 1.85 GHz, while n_+ changes from negative to positive. In Figure 5(c), from 1.80 GHz to 2.01 GHz, the loss factor of both RCP and LCP excitations (simulation) is low (< 0.5), while the loss factors of the measured data shown in Figure 5(d), from 1.60 GHz to 1.85 GHz, are higher, varying from 0.3 to 1.0. Some variations between the theoretical and measured results are caused by the limited

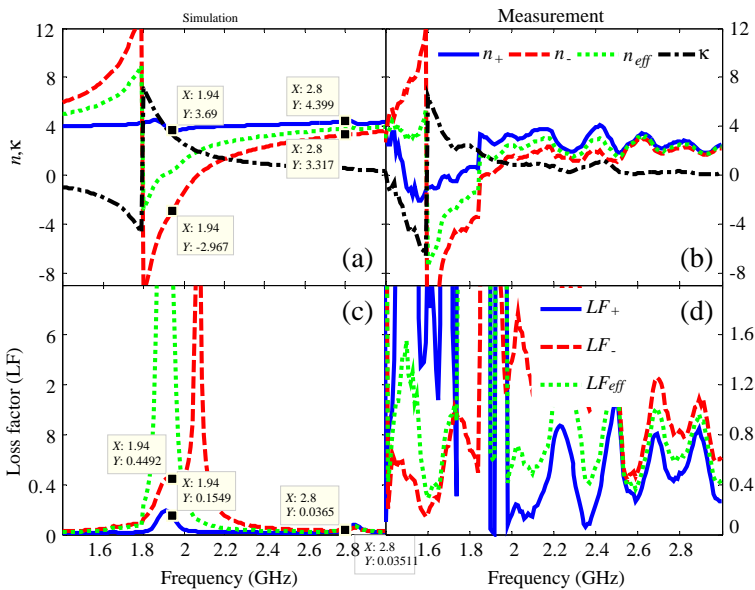


Figure 5. (Color online) simulation and experiment results of 3D planar triple helix: (a) and (b) refractive and chirality index, and (c) and (d) loss factor of RCP and LCP waves.

dimensions of the fabricated prototype [26], fabrication imperfections, as well as accuracy limit of the measuring instruments. However, we may conclude that there is low loss transmission for both excitations within the operating frequency. The RCP and LCP waves propagate through these triple helix stacks with a different refractive index stating circular birefringence. For instance, at 2.01 GHz, n_+ is 3.79 with the transmission amplitude of -1.96 dB, and n_- is -1.09 with the RCP amplitude of -3.03 dB.

Figure 6 illustrates the transmission of the RCP and LCP waves through a wedge constructed from the designed triple helix stack. Two frequencies where both LCP and RCP waves propagate with low loss, 1.94 GHz (located within the transmission bandwidth) and 2.8 GHz, marked in Figure 5(a) and Figure 5(c), are selected to investigate the circular birefringence. A TEM linear polarization wave is lunched from the base to the top of the wedge along \bar{k} , as shown in Figure 6. The wedge dimension is set as 8 unit cells (height, h) \times 3 unit cells (width, w) or 150 mm \times 56.25 mm. In order to build an 8.5° wedge, 9 unit cells have to be placed along the propagation direction (wedge length) of the short side (A), and 12 unit cells along the propagation direction of the long side (B). The adjacent cells are separated by 0.5 mm; therefore the short side is 65.39 mm and the long side is 87.71 mm. Hence, the 8.5° wedge, $\tan^{-1}((A - B)/w)$, is constructed.

At 1.94 GHz (Figure 5(a)), n_+ and n_- are 3.69 and respectively

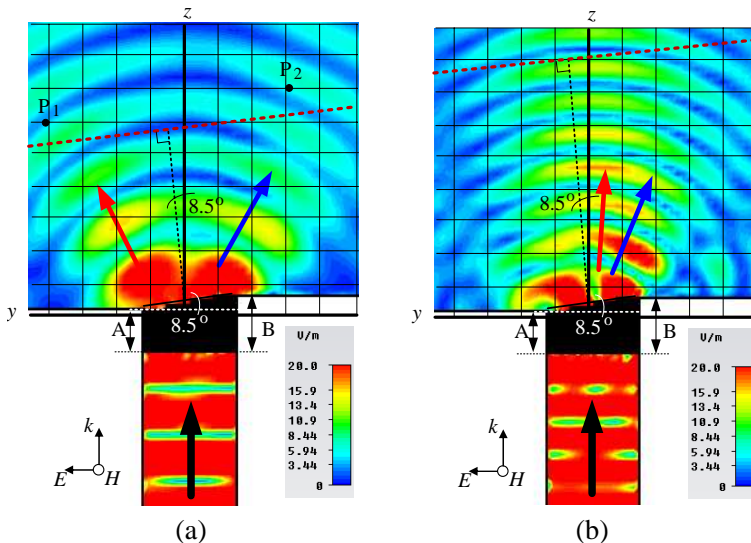


Figure 6. Transmission of RCP and LCP waves through triple helix wedge at (a) 1.94 GHz and (b) 2.80 GHz.

-2.97. Based on Snell’s law and the wedge angle of 8.5° , the RCP wave will propagate to free space with the outgoing angle of $+32.88^\circ$ (blue arrow), with respect to the normal line of the outgoing surface, while the LCP wave will travel out with a -25.91° outgoing angle (red arrow). The direction of the two transmitted waves in Figure 6(a) supports the previous results shown in Figure 5(a). This confirms that the RCP and LCP waves are split with a 58.79° wide angle. Another example is at 2.80 GHz, where n_+ and n_- are 4.40 and 3.32, respectively (Figure 5(a)). Based on Snell’s Law, the transmitted RCP and LCP waves will propagate through the chiral wedge with an outgoing angle of 40.34° and respectively 29.24° , therefore having the splitting angle of 11.10° . The direction of the two waves presented in Figure 6(b) supports the refractive index values retrieved earlier.

To further investigate the polarization of the outgoing wave within the operating frequency of 1.94 GHz, electric field components, E_x and E_y at points P_1 and P_2 marked in Figure 6(a) are collected. Point P_1 (0, 206 mm, -300 mm) and P_2 (0, -158 mm, -350 mm) lay outside the far-field region on the -25.91° and $+32.88^\circ$ line, respectively. The amplitude (A_1, A_2) and phase (θ_1, θ_2) of E_x and E_y at point P_1 and P_2 are presented in Table 1. The phase difference between E_x and E_y , θ , is determined by $\theta_1 - \theta_2$. Since $A_1 \neq A_2$ and $\theta \neq 0$, or $\theta \neq \pi$, the outgoing wave is proved to be elliptically polarized [18, 19]. If the angle θ is arbitrary and it is not equal to $\pm\pi/2$, the major axis (E_x) and minor axis (E_y) of the ellipse will be rotated with the rotation angle of $(1/2) \tan^{-1}(2A_1A_2 \cos \theta / (A_1^2 - A_2^2))$ [27, 28]. If $\sin(\theta) > 0$, the rotation is counterclockwise or left-elliptically polarized, and clockwise or right-elliptically polarized when $\sin(\theta) < 0$ [29]. At the observed points, P_1 and P_2 , $\sin(\theta)$ is negative and positive, respectively, stating that the outgoing waves at point P_1 and P_2 are left-handed and right-handed. Figure 7 illustrates the left- and right elliptical polarization at points P_1 and P_2 at 1.94 GHz.

Table 1. E_x and E_y , rotation of electric field, and polarization configuration of the outgoing wave at point P_1 and P_2 at 1.94 GHz.

Positions	E_x		E_y		θ ($^\circ$)	$\sin(\theta)$	Rotation angle	Polarization Configuration
	A_1 (V/m)	θ_1 ($^\circ$)	A_2 (V/m)	θ_2 ($^\circ$)				
P_1	0.80	129.50	6.41	-84.67	214.17	-0.56	5.92°	Left/Elliptical 
P_2	0.77	-118.58	6.70	-156.08	37.23	0.61	-5.25°	Right/Elliptical 

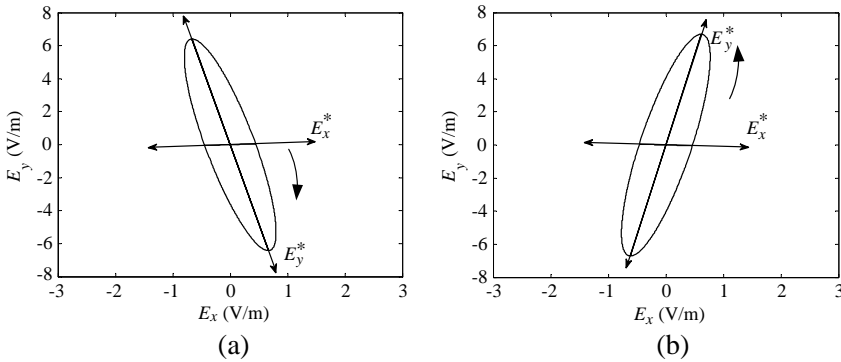


Figure 7. Left- and right-elliptical polarization at point (a) P_1 and (b) P_2 at 1.94 GHz.

4. CONCLUSIONS

Simple three-dimensional artificial triple helices are designed to generate circular birefringence with low loss in microwave regimes. High chirality is found within the transmission bandwidth where low loss transmission of RCP and LCP excitation waves propagate through triple helix stacks with a different refractive index. At 1.94 GHz, a wide splitting angle of 58.79° from the RCP wave with $n_+ = 3.69$ and from the LCP wave with $n_- = -2.97$ is obtained. The measurement results confirm the simulation results. The results of the wedge structure also support this design.

ACKNOWLEDGMENT

This project is financially supported by the Thailand Research Fund (RSA5480010) and the Faculty of Engineering, Khon Kaen University, Thailand. We also thank the Office of the National Broadcasting and Telecommunications Commission (NBTC) for funding the CST Microwave Studio[®] software applied in the simulations.

REFERENCES

1. Lakhtakia, A., V. K. Varadan, and V. V. Varadan, *Lecture Note in Physics: Time-harmonic Electromagnetic Fields in Chiral Media*, Springer, Heidelberg, Berlin, 1989.
2. Xia, Y., Y. Zhoua, and Z. Tang, "Chiral inorganic nanoparticles:

- Origin, optical properties and bioapplications,” *Nanoscale*, Vol. 3, 1374–1382, 2011.
3. Lindell, I. V., A. H. Sihvola, S. A. Tretyakov, and A. J. Viitanen, *Electromagnetic Waves in Chiral and Bi-isotropic Media*, Artech House Publishers, Boston, MA, 1994.
 4. Wongkasem, N. and A. Akyurtlu, “Light splitting effects in chiral metamaterials,” *J. Opt.*, Vol. 12, 035101, 2010.
 5. Sonsilphong, A. and N. Wongkasem, “Novel technique for high refractive index manifestation,” *International Conference on Electromagnetics in Advanced Applications*, 536–539, 2011.
 6. Wongkasem, N., A. Akyurtlu, J. Li, A. Tibolt, Z. Kang, and W. D. Goodhue, “Novel broadband terahertz negative refractive index metamaterials: Analysis and experiment,” *Progress In Electromagnetics Research*, Vol. 64, 205–218, 2006.
 7. Gansel, J. K., M. Thiel, M. S. Rill, M. Decker, K. Bade, V. Saile, G. V. Freymann, S. Linden, and M. Wegener, “Gold helix photonic metamaterial as broadband circular polarizer,” *Science* Vol. 325, 1513, 2009.
 8. Gansel, J. K., M. Wegener, S. Burger, and S. Linden, “Gold helix photonic metamaterials: A numerical parameter study,” *Optics Express*, Vol. 18, 1059, 2010.
 9. Yang, Z. Y., M. Zhao, P. X. Lu, and Y. F. Lu, “Ultrabroadband optical circular polarizers consisting of double-helical nanowire structures,” *Optics Letters*, Vol. 35, 2588–2590, 2010.
 10. Yang, Z. Y., M. Zhao, and P. X. Lu, “How to improve the signal-to-noise ratio for circular polarizers consisting of helical metamaterials?” *Optics Express*, Vol. 19, 4255–4260, 2011.
 11. Ma, X., C. Huang, M. Pu, C. Hu, Q. Feng, and X. Luo, “Multi-band circular polarizer using planar spiral metamaterial structure,” *Optics Express*, Vol. 20, 16050–16058, 2012.
 12. Ma, X., C. Huang, M. Pu, Y. Wang, Z. Zhao, C. Wang, and X. Luo, “Dual-band asymmetry chiral metamaterial based on planar spiral structure,” *Appl. Phys. Lett.*, Vol. 101, 161901, 2012.
 13. Wang, B., T. Koschny, and C. M. Soukoulis, “Wide-angle and polarization independent chiral metamaterials absorbers,” *Phys. Rev. B*, Vol. 80, 033108, 2009.
 14. Plum, E., J. Zhou, J. Dong, V. A. Fedotov, T. Koschny, C. M. Soukoulis, and N. I. Zheludev, “Metamaterial with negative index due to chirality,” *Phys. Rev. B*, Vol. 79, 035407, 2009.
 15. Zhou, J., J. Dong, B. Wang, T. Koschny, M. Kafesaki, and C. M. Soukoulis, “Negative refractive index due to chirality,” *Phys.*

- Rev. B*, Vol. 79, 121104(R), 2009.
16. Li, Z., R. Zhao, T. Koschny, M. Kafesaki, K. B. Alici, E. Colak, H. Caglayan, E. Ozbay, and C. M. Soukoulis, "Chiral metamaterials with negative refractive index based on four 'U' split ring resonators," *Appl. Phys. Lett.*, Vol. 97, 081901, 2010.
 17. Zhao, R., L. Zhang, J. Zhou, T. Koschny, and C. M. Soukoulis, "Conjugated gammadion chiral metamaterial with uniaxial optical activity and negative refractive index," *Phys. Rev. B*, Vol. 83, 035105, 2011.
 18. Wang, B., J. Zhou, T. Koschny, and C. M. Soukoulis, "Nonplanar chiral metamaterials with negative index," *Appl. Phys. Lett.*, Vol. 94, 151112, 2009.
 19. Wongkasem, N., C. Kamtongdee, A. Akyurtlu, and K. Marx, "Artificial multiple helices: EM and polarization properties," *J. Opt.*, Vol. 12, 075102, 2010.
 20. Sonsilphong, A. and N. Wongkasem, "Three-dimensional artificial double helices with high negative refractive index," *J. Opt.*, Vol. 14, 105103, 2012.
 21. Raos, G., "Degrees of chirality in helical structures," *Macromol. Theory Simul.*, Vol. 11, 739–750, 2002.
 22. Green, M. M., N. C. Peterson, T. Sato, A. Teramoto, R. Cook, and S. Lifson, "A helical polymer with a cooperative response to chiral information," *Science*, Vol. 268, 1860–1866, 1995.
 23. Sonsilphong, A. and N. Wongkasem, "Transmission properties in chiral metamaterials," *International Journal of Physical Sciences*, Vol. 7, No. 21, 2829–2837, 2012.
 24. CST Microwave Studio: <http://www.cst.com/>.
 25. Wang, B., J. Zhou, T. Koschny, M. Kafesaki, and C. M. Soukoulis, "Chiral metamaterials: Simulations and experiments," *J. Opt. A: Pure Appl. Opt.*, Vol. 11, 114003, 2009.
 26. Ranga, Y., L. Matekovits, K. P. Esselle, and A. R. Weily, "Multi-octave frequency selective surface reflector for ultrawideband antennas," *IEEE Antennas and Wireless Propagat. Letters*, Vol. 10, 219–222, 2011.
 27. Balanis, C. A., *Advanced Engineering Electromagnetic*, John Wiley & Sons, 1989.
 28. Orfanidis, S. J., "Electromagnetic waves and antennas," Online URL: <http://www.ece.rutgers.edu/~orfanidi/ewa/>.
 29. "IEEE standard definitions of terms for antennas," IEEE Std 145-1983, Revised IEEE Std 145-1993, 1993.